ENCIT 2018

ABCM Associação Brasileira de Engenharia e Ciências Mecânicas

17th Brazilian Congress of Thermal Sciences and Engineering
November 25th-28th, 2018, Águas de Lindóia, SP, Brazil

ENCIT2018-0234
OPTIMIZATION OF DOUBLE PIPE-HEAT EXCHANGER WITH SINGLE SEGMENTAL PERFORATED BAFFLES

Andrey Barbosa Colaço
Flavia Bernardo
Marcos Batistella Lopes
Viviana Cocco Mariani
Department of Mechanical Engineering, Pontifical Catholic University of Paraná, R. Imaculada Conceição, 1155, Curitiba, Brazil
colaco.andrey@gmail.com, fla.bernardo@gmail.com, marcos.batistella.lopes@gmail.com, viviana.mariani@pucpr.br
Leandro dos Santos Coelho
Industrial and Systems Engineering Graduate Program, Pontifical Catholic University of Paraná, R. Imaculada Conceição, 1155, Curitiba, Brazil
leandro.coelho@pucpr.br
Mohamed Reda Salem
Faculty of Engineering at Shoubra, Benha University, Shoubra St., 108, Cairo, Egypt
mohamed.abdelhamid@feng.bu.edu.eg

Abstract. *This work represents the results of optimization in a convective heat transfer and pressure drop of water flow in the annulus-side of horizontal double pipe heat exchangers. Therefore, the objective of this article is the application of differential evolution algorithm (DE) to solve mono-objective problems considering five cases with/without Single Segmental Perforated Baffles (SSPBs), which are fabricated with different holes spacing, void, cut and pitch ratios, which depends of the space between the holes (S – [3;6]), the diameter of the holes ($d_h - [1;4]$) and the dimension of cut region (H – [3.35;10.05]). To be a successful heat transfer enhancement tool, the rise in convective heat transfer given due to existing perforated baffles in heat exchangers should be higher than the rise in the fluid pressure drop at same pumping power. The objective function is maximize the thermal performance index (TPI), which is determined using Nusselt ratio and friction ratios that are calculated using the values obtained for existing perforated baffles and no baffles. The results revealed that numerical study is capable to increase the efficiency of the heat exchanger. Eleven cases were studied with an improvement in efficiency. CFD analysis showed the accuracy of the DE approach to optimize the heat exchanger performance.*

Keywords: *Perforated baffles, Heat exchanger optimization, Thermal performance, Friction factor, Differential Evolution algorithm*

1. INTRODUCTION

A heat exchanger is a device that is used to transfer thermal energy (enthalpy) between two or more fluids, between a solid surface and a fluid, or between solid particulates and a fluid, at different temperatures and in thermal contact. The basic principle of a double-pipe heat exchanger is two fluids flow at different temperatures separated by a wall. Tubular heat exchangers in their various forms are probably the most widespread and commonly used equipment in the process industries. They are essential equipment for all the major industries like chemical and petrochemical plants, oil refineries, power plants and metallurgical operations. The reasons for this general acceptance is that they are relatively simple to manufacture, and have multi-purpose application possibility when compared with other types of heat exchangers.

In addition to the heat transfer studies, (CFD) computational fluid dynamics is being increasingly used because of the developments in the computational power as well as numerical techniques. Tubular heat exchanger could be baffled or unbaffled. Baffles are used for directing the flow inside the shell from the inlet to the outlet while maintaining effective circulation of the shell side fluid hence providing effective use of the heat transfer area. In the double pipe heat exchanger the baffles provide support for the tube, enable a desirable velocity to be maintained for the annulus-side fluid flow, and prevent the tube from vibrating. Baffles also guide the annulus-side flow to move forward across the tube, increasing fluid velocity and heat transfer coefficient. The most commonly is the single segmental perforated baffles (SSPB), heat transfer is improved as the baffles guide the annulus side fluid to flow in a zigzag pattern between the tube, which enhances the turbulence intensity and the local mixing. Figure 1 below shows the schematic drawing of a double pipe heat exchanger.

Donohue (1949) experimentally investigated the heat transfer phenomenon in unbaffled and baffles heat exchangers and explained that in an unbaffled shell, fluid flows parallel to tube is similar to the flow inside a tube. He evaluated the factors influence heat transfer coefficient and pressure drop.

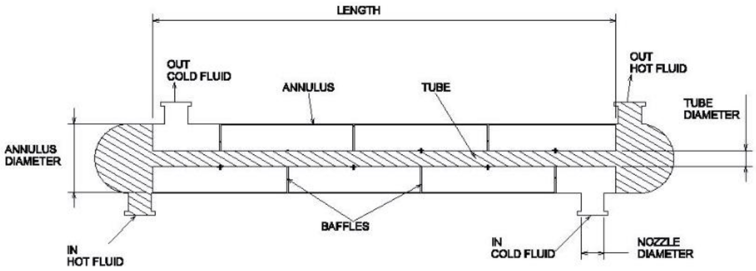

Figure 1. Schematic drawing of a double pipe heat exchanger.

Several works relate to the study of tubular heat exchanger with and without baffles have been developed in the past few decades. A few of numerical studies dealing with these problems are summarized in Table 1, which presents some strong points of each research. Some of experimental studies have been developed and summarized in Table 2.

Table 1. Summary of some numerical studies related to tubular heat exchanger

References	Type Tubular	Turbulence Model	Mesh	Boundary conditions		Parameters evaluated
				In	out	
Maakoul *et al.*	Baffled	k–ε	unstructured tetrahedral grid	Velocity-Inlet	Pressure outlet = zero [Pa]	Nusselt and Reynolds numbers, mass flow, Heat transfer coefficient
Pal *et al.*	Both	k–ε, k–ω SST k–ω	3D tetrahedral grid	Dirichlet-Vel. Neumann-Pressure	Neumann	Nusselt and Reynolds numbers, temperature profile
Guo-Yan Zhou *et al.*	Baffled	k–ε	Structured tetrahedral grid	238K	Constant temperature in inner tubes T=307K	Nusselt and Reynolds numbers,Pressure drop
Mellal *et al.*	Baffled	k–ε	3D tetrahedral grid	293.15 K, Velocity-inlet	353.15 K in inner tube and pressure outlet	Nusselt and Reynolds numbers, friction factor
Labbadlia *et al.*	Unbaffled	k-ω SST	Unstructured tetrahedral grid, hybrid	velocity 1.252 m/s	-	Influence of Tube Arrangement and angle
Ozden and Tari	Baffled	variations of k–ε	Quadrilateral elements in surface and tetragonal-hybrid elements in vol.	300K inlet	Constant temperature in inner tubes T=450K	Number and space of baffles, pressure drop and heat transfer ratio
Paul et al.	Unbaffled	k–e, k–ω, SST, LRR-IP	Structured, non-orthogonal, non-uniform, boundary fitted grids	0.34 m/s	Pressure Average outlets	Turbulence model influence and Reynolds number
Lei *et al.*	Baffled	k–ε	Unstructured tetrahedral grid	333 K temperature inlet	Constant temperature in inner tubes T=298K	Mass flow and pressure drop, heat transfer coefficient

Table 2. Summary of some experimental studies related to tubular heat exchanger

References	Baffles	Fluid	Dimensions Dc (mm)	L (mm)	Dit (mm)	Det (mm)	N° of Tubes	Parameters Evaluated
Aicher and Kim (1997)	Unbaffled	Water	34-50	920–2000	11-37	13-40	1	Influence of cross flow, Nusselt and Reynolds
Gao *et al.*	Baffled	Water/ Oil	313	1184-3075	25	27	16-24	Friction factor, heat transfer ratio, coefficient of heat transfer, Reynolds
Wen *et al.*	Baffled	Water	250	2000	-	19	45	Thermal performance factor, pressure loss, mass flow, coefficient of heat transfer
Yang *et al.*	Baffled	Water/ Oil	124	765	-	50	212	Nusselt, Reynolds, Friction Factor, coefficient of heat transfer
Aicher and Kim. (1998)	Unbaffled	Water	34– 150	920–2000	6–37	8–40	1–91	Influence of cross flow, Nusselt and Reynolds
Salem *et al.*	Both	Water	50.8	1200	26	28	1	Reynolds, Nusselt, Friction factor
Uzzan *et al.*	Unbaffled	Water/ Milk	20.9	3780	-	10.9	1	Distribution of temperature, coefficient of heat transfer
Paul *et al.*	Unbaffled	Water	191	2500	-	25.4	12	Influence of turbulence models and Reynolds
You *et al.*	Baffled	Water	100	2000	12	14	14	Pressure loss, Reynolds, Nusselt
Zhang *et al.*	Baffled	Water	325-313	1194	15	19	97	Friction factor, heat transfer ratio, coefficient of heat transfer, Reynolds, Nusselt and pressure loss

Aicher and Kim (1997) experimentally investigated the shell side heat transfer of 32 different types of heat exchangers. From the experimental results it can be confirmed that the influence of the tube pitch is small enough to be neglected in shell-and-tube heat exchangers used in real processes. The heat transfer rate of the longitudinal flow can be calculated from the correlation for turbulent flow in concentric annular ducts by inserting the porosity instead of the ratio of tube to shell diameter. The influence of the cross flow in the nozzle region increases with decreasing length of the heat exchangers. The heat transfer coefficients in the nozzle region are determined by comparing the overall heat transfer coefficients of the heat exchangers with that calculated from the correlation for the longitudinal flow. The results show that the heat transfer coefficient in the nozzle region is 40 % greater than that in the parallel region, if the length of the apparatuses is about 30 times the hydraulic diameter.

This work was extended further by Aicher and Kim (1998) by using the double pipe heat exchangers. They found out that the influence of cross flow is higher in the case of shorter heat exchangers. Also, as the ratio of free cross sectional area of nozzle to free cross sectional area of shell side decreases the effect of cross flow is more prominent. They developed a correlation to describe the Nusselt number for highly turbulent flow Re > 10.000.

Uzzan, *et al.*, 2004 develop an analytical solution for steady-state temperature profiles within a double pipe (concentric cylinders) heat exchanger with counter current flow. The results were compared with the available experimental data.

In previous studies, Salem, *et al.*, 2017 constructed twelve concentric tube heat exchangers of counter-flow configurations. One without any baffles, while eleven heat exchangers are fabricated with different SSPBs holes spacing ratio (Ψ) as in Eq. (1), void ratio (Φ) as in Eq. (2), cut ratio (δ) as in Eq. (3), pitch ratio (λ) as in Eq. (4) and inclination angle (θ). The SSPBs are formed from 0.6 mm thick copper sheet and a laser is used during cutting and drilling process.

All baffles have a circular shape of the same diameter of the heat exchanger annular pipe; 50.8 mm except the inclined SSPBs which have a parabolic shape to keep the same cut ratio.

The Figure 2 below shows the schematic drawing of the Single Segmental Perforated Baffles (SSPBs), where S is the space between the holes, d_h is the diameter of the holes, and H is the dimension of cut region.

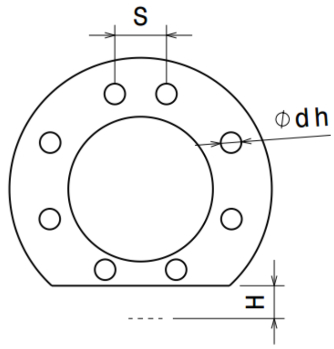

Figure 2. Schematic drawing of the Single Segmental Perforated Baffles (SSPBs).

$$\Psi = \frac{S}{d_h} \tag{1}$$

$$\Phi = \frac{N_h \frac{\pi}{4} (d_h)^2}{\frac{\pi}{4} \left(d_{an,in}{}^2 - d_{t,out}{}^2\right) - A_w} \tag{2}$$

$$\delta = \frac{H}{d_{an,in}} \tag{3}$$

$$\lambda = \frac{P_b}{d_{an,h}} \tag{4}$$

where, N_h is the number of holes, $d_{an,in}$ is the inner diameter annular, $d_{t,out}$ is the outer diameter of tube, A_w is the area of the baffle window, P_b is the pich of baffles and L is the length of the heat exchanger.

In this work they developed correlations through power regression models to predict the annulus average Nusselt number ($\overline{Nu}_{an}$), as in Eq. (5), and its Fanning friction factor (f_{an}), as in Eq. (6), with using SSPBs inside. The annulus average Nusselt number is correlated as a function of annulus-side Reynolds and Prandtl numbers, baffles spacing ratio, void ratio, cut ratio, pitch ratio and inclination angle in degrees as follows:

$$\overline{Nu}_{an} = 0.0015\ Re_{an}^{1.25}\ Pr_{an}^{1.03}\ \Psi^{0.35}\ \Phi^{0.31}\ \delta^{-0.46}\ \lambda^{-0.77}\ \left(\frac{\theta}{90}\right)^{0.21} \tag{5}$$

And for annulus-side Fanning friction factor is obtained as follows:

$$f_{an} = 3.3\ Re_{an}^{-0.58}\ \Psi^{0.22}\ \Phi^{0.22}\ \delta^{-0.3}\ \lambda^{-0.5}\ \left(\frac{\theta}{90}\right)^{0.17} \tag{6}$$

Prant annular (Pr_{an}) is defined as the ratio of momentum diffusivity to thermal diffusivity $\left(\frac{C_p \mu}{k}\right)$. Where C_p is specific heat, μ is dynamic viscosity and k is thermal conductivity.

2. METHODOLOGY

The present study improves the performance of a double pipe heat exchanger with segmental perforated baffles using those correlations Eqs. (5) and (6). To be a successful heat transfer enhancement tool, the rise in convective heat transfer given due to existing perforated baffles in heat exchangers should be higher than the rise in the fluid pressure drop at same pumping power. So, the objective function is the Thermal Performance Index (TPI), which was proposed by Salem, *et al.*, 2017 and is determined using Nusselt ratio and friction ratio that are calculated using the values obtained for existing perforated baffles and no baffles as fallows in Eq. (7):

$$TPI = \frac{\overline{Nu}_{an\ \ baffles}\ /\ \overline{Nu}_{an,\ \ no\, baffles}}{\left(f_{an,\ \ baffles}\ /\ f_{an,\ \ no\, baffles}\right)^{1/3}} \tag{7}$$

With this purpose, the differential evolution algorithm was used to solve the mono-objective problem. After optimization of the values of spacing ratio (Ψ); void ratio (Φ); cut ratio (δ) and pitch ratio (λ), a new baffle is proposed and a CFD model is developed in a commercial CFD package, ANSYS CFX to verify the better performance of the heat exchanger.

2.1 Mathematical equations

The flow is assumed to be in steady-state, 3-dimensional, incompressible and turbulent. The thermophysical properties of the water in the annulus and internal tube are considered constant.

The governing equations including the mass conservation (continuity), momentum conservation, and energy conservation equations are as the following:

Continuity equation:

$$\frac{\partial u_i}{\partial x_i} = 0 \tag{8}$$

Momentum equation:

$$\frac{\partial u_i u_j}{\partial x_i} = -\frac{1}{\rho}\frac{\partial p}{\partial x_i} + \frac{\partial}{\partial x_j}\left((v + v_{turb})\left(\frac{\partial u_i}{\partial x_j} + \frac{\partial u_j}{\partial x_i}\right)\right) \tag{9}$$

Energy equation:

$$\frac{\partial u_i T}{\partial x_i} = \rho\frac{\partial}{\partial x_i}\left(\left(\frac{v}{Pr} + \frac{v_t}{Pr_{turb}}\right)\frac{\partial T}{\partial x_i}\right) \tag{10}$$

The Turbulence model k-ω SST (Shear Stress Transport) used could be represented by

$$\frac{\partial(\rho k)}{\partial t} + \vec{\nabla}.\{\rho k U\} = \nabla[(\mu + \sigma_k \mu_t)\nabla k] + P_k - \beta' \rho k \omega \tag{11}$$

$$\frac{\partial(\rho\omega)}{\partial t} + \vec{\nabla}.\{\rho\omega U\} = \nabla[(\mu + \sigma_{\omega 1}\mu_t)\nabla\omega] + (1 - F_1)2\,\rho\,\sigma_{\omega 2}\,\frac{1}{\omega}\,\nabla k\,\nabla\omega + \alpha_3\frac{\omega}{k}\,P_k - \beta\rho\omega^2 \tag{12}$$

where, $\sigma_{\omega 1}$ is a constant equal to 2; F_1 is a mix function; $\sigma_{\omega 2}$ is a constant equal to $\frac{1}{0.856}$ (Ansys, 2012).

The definition for the y^+ variable that appears in the post processor is given by the standard definition generally used in CFD (Ansys, 2012) as follow,

$$y^+ = \frac{\sqrt{\tau_\omega/\rho}\,\Delta n}{v} \tag{13}$$

where, Δn is the distance between the first and second grid points off the wall.

2.2 Differential Evolution

The differential evolution (DE) is a bioinspired algorithm based in population denominated optimization metaheuristic. The classic algorithm of DE is the same of genetic algorithm, but it is faster than its predecessor (Pinto, 2016). The optimization metaheuristics are widely recognized as efficient approaches to solve many optimization problems that do not have exact solution (Boussaïd *et al.*, 2013). According Das, *et al.*, 2009 in recent years, many approaches of DE have been highlighted in optimization and in some cases even better results than many other bioinspired algorithms.

Many applications have used the DE algorithm to search for solutions, as in the case of the optimization of the trajectory of a satellite (Ghosh, Chattopadhyay, 2015). In an extend way, the DE algorithm can be interpreted by the following steps, assuming that the search for the global optimization point is a real parameter in the space R^D:

i. The initial population must be within the lower and upper bounds of each project variable and initialized at random, as shown in Eq. (14)

$$x_{i,g} = x_{i,L} + rand_{g,i}[0,1](x_{i,U} - x_{i,L}) \tag{14}$$

where, i is the individual, g is the generation, $x_{i,L}$ are lower limits of the project variable and e $x_{i,U}$ are lower limits of the project variable and $rand_{g,i}[0,1]$ is the random number generated with uniform distribution in the interval 0 and 1.

ii. Then, the initial population generated must be evaluated by an objective function;

iii. After being evaluated, the population must undergo mutation (DE strategy) using a difference vector and resulting in the perturbation vector. The Eq. (5) show the perturbation vector calculation for the strategy *rand-to-best*/1/*bin*:

$$v_{i,g} = x_{i,g} + F\left(x_{r_1^i,g} - x_{i,g}\right) + F\left(x_{r_2^i,g} - x_{r_3^i,g}\right) \tag{15}$$

where, $x_{r_1^i}$, $x_{r_2^i}$ e $x_{r_3^i}$ are randomly selected vectors of the current population, the indices r_1^i, r_1^i e r_3^i are random integers chosen between $[1, NP]$, F is the weighting factor or weight applied to the difference vector given the Eq. (16) and $v_{i,g}$ is perturbation vector;

$$F = F_m rand(1) + F_m \tag{16}$$

iv. After mutation, the binomial cross of the population must be applied to result in the new diversified generation, as show in Eq. (17):

$$u_{i,g}^{j} = \begin{cases} v_{i,g}\ se\ rand_j\ (0,1) \leq Cr\ ou\ j = j_{rand} \\ x_{i,g}\ caso\ contrário \end{cases} \tag{17}$$

where, *Cr* is the crossing coefficient, and $j = 1,2, \dots D$.

v. And finally, the next step is the selection for the new generation. In the DE the whole population competes with each other, that is, the one with the best value of the objective function is selected for the next generation, as show in Eq.(18):

$$x_{i,g+1} = \begin{cases} u_{i,g}\ \text{se}\ f(u_{i,g}) \leq f(x_{i,g}) \\ x_{i,g}\ caso\ contrário \end{cases} \tag{18}$$

where, $f(x)$ is the objective function will be minimized.

The routine i. until the routine v. must be repeated until it reaches the stop criterion. According by Das and Suganthan (2011), the stop criterion can be: 1) iteration numbers (gen_{max}); 2) while the best *fitness* of the population does not change appreciably after successive iteration; and 3) achieve a predefined objective function value. For optimization of the inverse method was used the MATLAB© code. It was run one experiment for each case and for the stopping criterion was using equal to 1000. The Table 3 shown the DE parameters used in simulations of this present study, as well as, the lower and upper boundary of the optimization variables, denoted by $x_{i,L}$ and $x_{i,U}$, respectively.

Table 3. DE parameters and lower and upper limit about optimization variables.

Parameter	Value
D	3
$x_{i,L}$,	[1 3 3.35]
$x_{i,U}$	[4 6 10.05]
NP	30
Cr	0.8
F_m	0.1

2.3 Domains and Mesh generation

The internal tube of all exchangers is a copper tube of 26 mm internal diameter and 28 mm external diameter. The annular side is made of tube with 50.8 mm internal diameter. The length of all heat exchangers annular pipes and their internal tube is 1200 mm.

For each model of heat exchangers studied, three domains are defined, two fluid domains (water in the inner tube and water in the annulus side) and one solid domain (tube). The computational domains are meshed with a mix of unstructured tetrahedral and wedge (Prism) grid as can be seen in Fig. 3. Near the tube and annular wall, the meshing consists of a boundary layer made up of structured cells which is result of the use of inflation layers. The number of layers used for inflations was 5; the growth rate was 1.2; maximum thickness equal 2.5 mm.

In order to mesh the heat exchanger, ANSYS CFX MESH software was used. A series of grid sensitivity tests were carried out to ensure that optimized computational mesh was obtained. Three sets of grids (~4.3 million, ~6.3 million and ~8.4 million elements) are computed. It was found a small difference in the rate of heat transfer between ~6.3 million and ~8.4 million, considering both convergent time and solution accuracy, so the grid system ~6.3 million elements was adopted. Table 4 shows a few characteristics of mesh grid.

Table 4. Summary of mesh characteristics

			Quality			
	Nodes	Elements	Skewness	Average	Standard Deviation	y^+ in annulus
Coarse	1,908,652	4,328,051	0.84650	0.15481	0.12114	1.51
Moderate	2,610,860	6,330,304	0.89275	0.15025	0.11207	1.46
Fine	3,294,168	8,392,301	0.84957	0.15426	0.11949	1.39

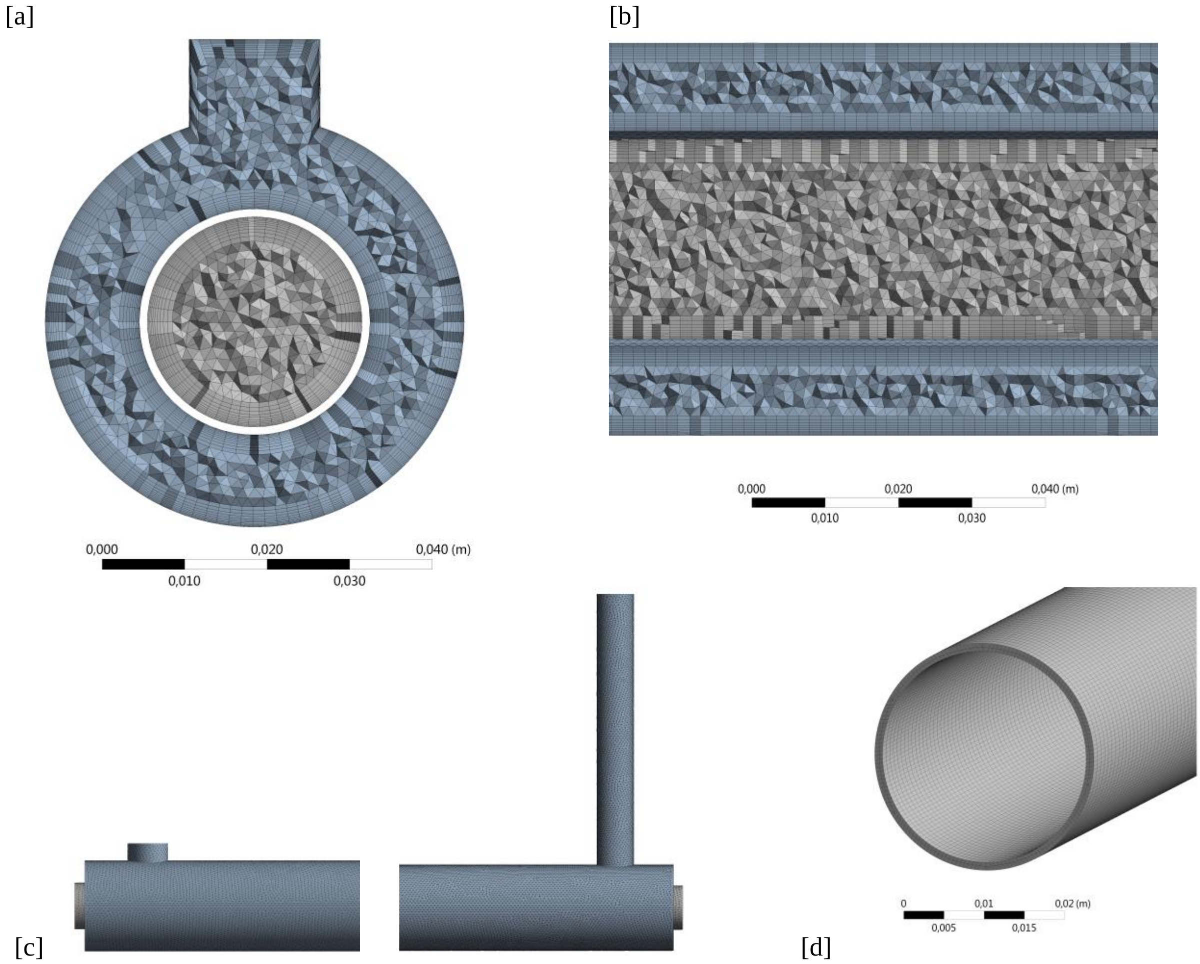

Figure 3. [a] Mesh grid generated in Fluid Domain, front view sectioned, [b] Mesh grid generated in fluid domain, side view sectioned, [c] Side view, [d] Solid Domain

2.4 Turbulence model

The $k-\ \omega$ based Shear-Stress-Transport (SST) model was used in this simulation. The $k-\ \omega$ SST was designed to give a highly accurate predictions of the onset and the amount of flow separation under adverse pressure gradients by the inclusion of transport effects into the formulation of the eddy-viscosity. This results in a major improvement in terms of flow separation predictions. The superior performance of this model has been demonstrated in a large number of validation studies, according to ANSYS, CFX Modeling Guide, 2012.

2.5 Boundary conditions

In this study, the momentum boundary condition of no slip and no penetration is used for all solid walls. The thermal boundary condition of zero heat flux is used for annulus outer walls (adiabatic), while wall of tube which contacted with water are solid-fluid interfaces as coupling heat transfer boundary condition. The inlets of water in annulus are set as velocity-inlet boundary condition from 0.100 kg/s to 0.306 kg/s with temperature of 293.15 K. The inlets of water in tube are set as velocity-inlet boundary condition with 0.134 kg/s fixed and temperature 323.15 K. The pressure-outlet boundary condition is set for opening with 0 Pa in tube and annular outlets, so the inlet pressure is equal to the pressure drop on both annulus and tube side.

2.6 Solution methodology

The computational work was carried out on the Ansys CFX solver. It is a fully three-dimensional CFD tool, based on the finite volume method. The steady state, Reynolds averaged Navier–Stokes equations of motion and the equation of energy were solved for an incompressible Newtonian fluid. The upwind scheme was used for discretization of convection terms.

2.7 Validation

One simple double-pipe heat exchanger is used in the model validation, and the current work is compared with the experimental study developed by Salem, *et al.* (2017).

The validation of the model in determining the heat transfer coefficients and friction factors is done by taking the results obtained in Ansys CFX solver and using the equations below. Thermophysical properties of the water in the annulus and internal tube are evaluated from Ralph (2001) and calculated at the bulk temperatures, $T_{an,ave}$ (average between $T_{an,in}$ and $T_{an,out}$) and $T_{t,ave}$ (average between $T_{t,in}$ and $T_{t,out}$) respectively.

The average Nusselt number for the annulus-side fluid ($\overline{Nu}_{an}$) can be obtained as,

$$\overline{Nu}_{an} = \frac{\bar{h}_{an}\, d_{an,h}}{k_{an}} \tag{19}$$

where $\bar{h}_{an}$ is the average convection heat transfer coefficient, $d_{an,h}$ is the hydraulic diameter of the annulus $d_{an,h} = d_{an,i} - d_{t,o}$ and k_{an} is the thermal conductivity. Eqs. (20)) and (21) show tube and annulus Reynolds numbers, respectively.

$$Re_t = \frac{4\,\dot{m}_t}{\pi\, d_{t,i}\mu_t} \tag{20}$$

$$Re_{an} = \frac{4\,\dot{m}_{an}\, d_{an,h}}{\pi\,\mu_{an}\,\left(d_{an,in}^2 - d_{t,o}^2\right)} \tag{21}$$

The Fanning friction factor (f_{an}) for the fluid in circulation inside the annulus side is calculated with Eqs. (22) and (23) show the axial velocity (u_{an}).

$$f_{an} = \frac{\Delta P_{an}\, d_{an,h}}{2\, L_{an}\ \ \rho_{an}\, u_{an}^2} \tag{22}$$

$$u_{an} = \frac{4\,\dot{V}_{an}}{\pi\,\mu_{an}\,\left(d_{an,in}^2 - d_{t,o}^2\right)} \tag{23}$$

Figures 4 and 5 show the results of these comparisons. All this validation is based in Case 1, which is with no baffles settings. It is indicated that the numerical model for both heat transfer and friction factor calculations are in good agreement with previous experimental studies. This good agreement in comparison reveals the accuracy of the numerical model.

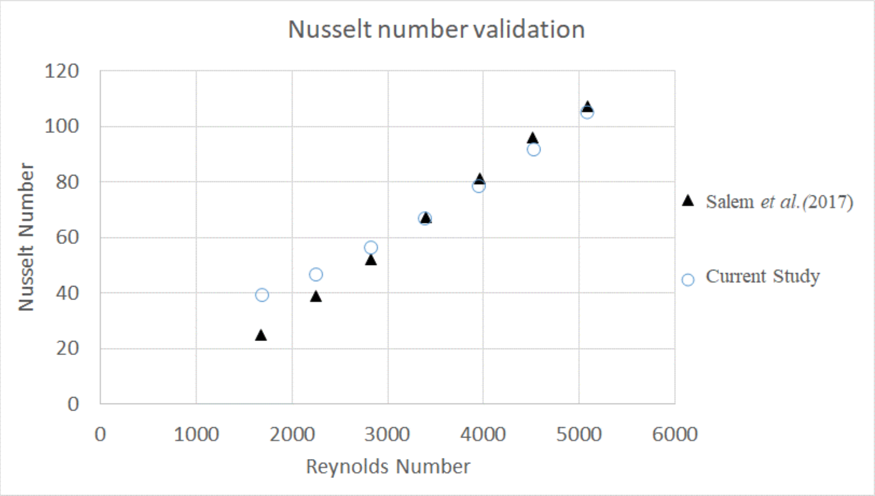

Figure 4. Nusselt Number Validation

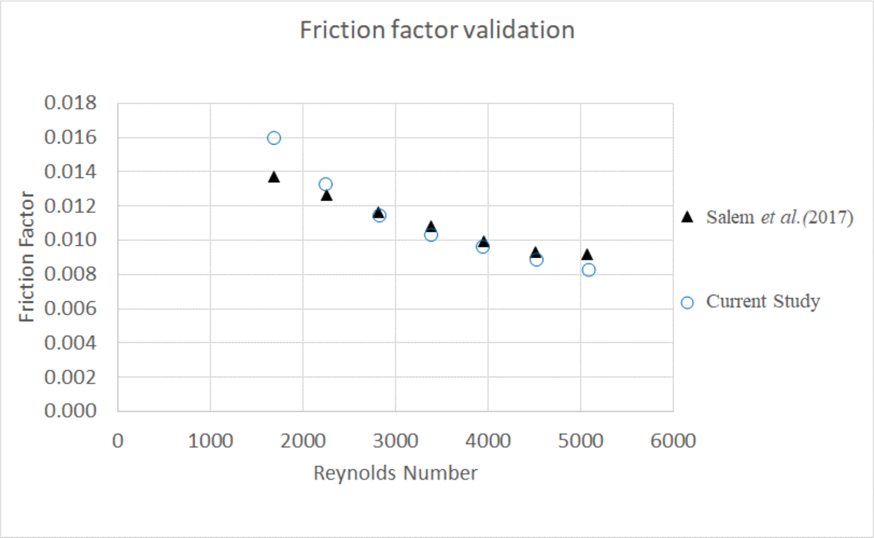

Figure 5. Friction Factor Validation

3. RESULTS AND DISCUSSION

The main objective of this study is to determine the better thermal performance index (TPI) for the range of flow using the value of space between the holes (S), diameter of the holes (d_h) and dimension of cut region (H) as described as:

$$f = \frac{\sum_0^j TPI}{j} \tag{24}$$

where, TPI is the thermal performance index given by Eq. (7) and j is the quantity into the range of the flow.

The best values of the parameters that obtain the best objective function f are shown in Table 5. Results reveled that for the optimized baffles configurations the thermal performance index (TPI) reached was better than previous studies. In Figure 6 can be seen a comparative between proposed baffle and previous studies for eleven cases, case one without baffle. It’s easy to see that the method adopted improved the performance of the heat exchanger, increasing Nusselt number and decreasing friction factor.

Table 5. Parameters and function objective values.

Cases	S	d_h	H	f
2	6.94	3.38	3.53	1.95476
3	7.00	2.78	3.52	2.067506
4	6.69	1.17	3.48	2.594863
5	7.00	3.95	3.53	1.958233
6	7.00	1.72	3.53	2.364749
7	7.00	2.78	3.52	2.043068
8	7.00	2.78	3.52	2.532857
9	6.99	3.31	3.53	2.184995
10	7.00	2.37	3.52	2.161735
11	6.88	2.61	3.52	1.882997
12	6.99	2.7	3.53	1.956483

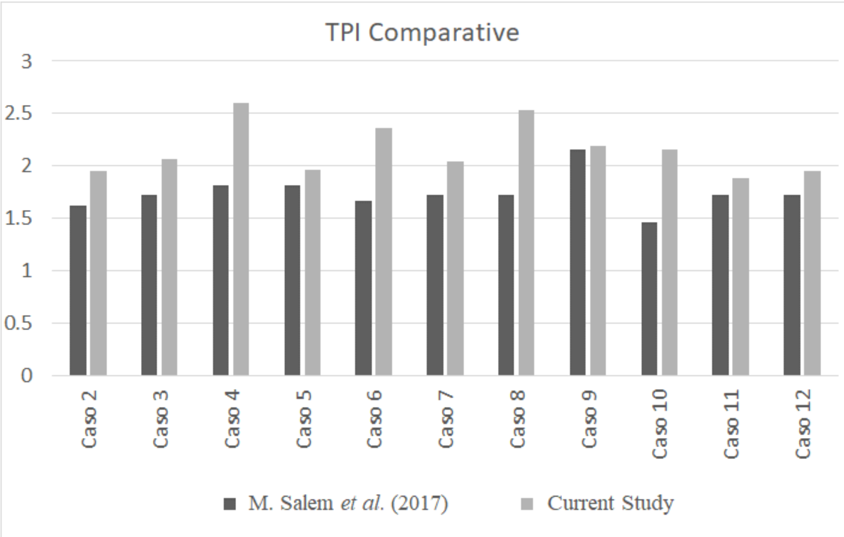

Figure 6. TPI Comparative

Figures above shows the results for the case 9, which was the better case founded by Salem, *et al.*, 2017. They proposed a correlation to predict de Nusselt number and friction factor, the results founded by numerical study are in agreement with experimental data. Figure 7 shows the temperature profile in annulus side. Figure 8 shows pressure profile in the annulus side, with these two results, it's possible to calculate the TPI. Figure 9 shows the velocity profile in the exit of the heat exchanger the exit must be length enough to allow a fully developed velocity profile.

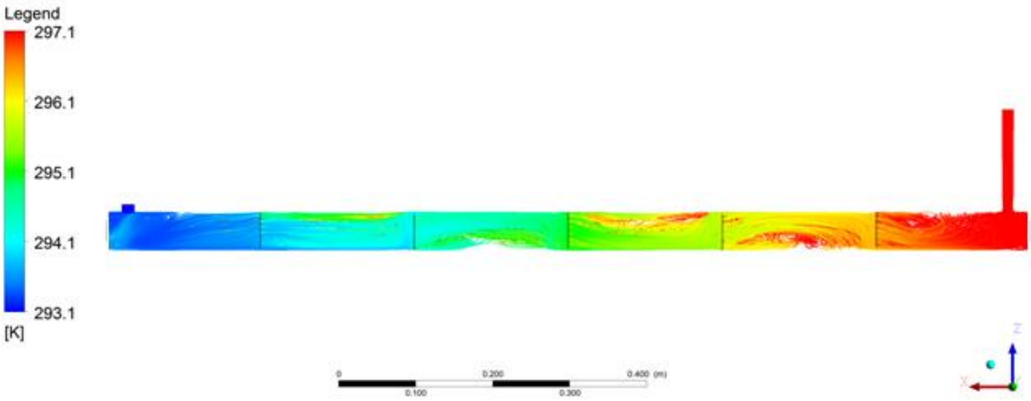

Figure 7. Temperature profile in annulus side

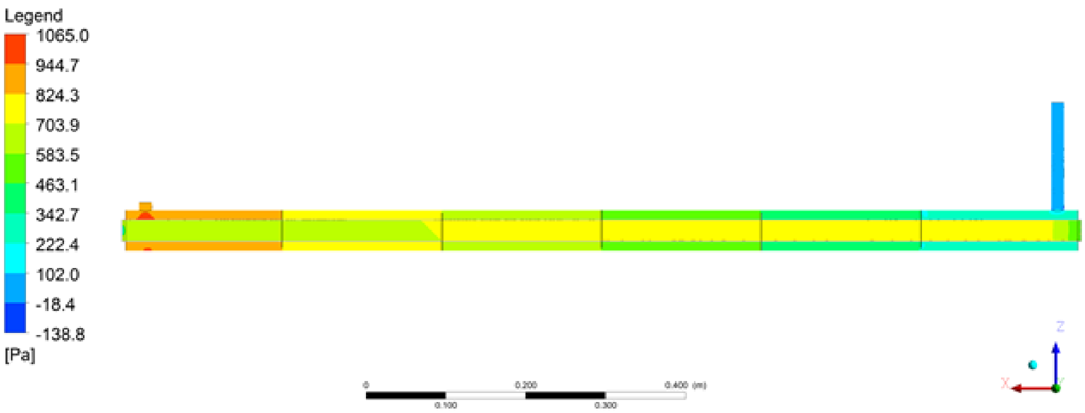

Figure 8. Pressure profile

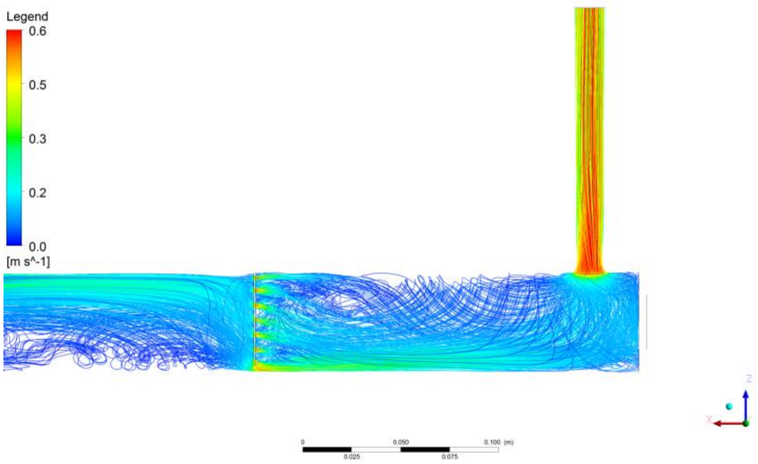

Figure 9. Velocity profile in exit of the heat exchanger

To have a comparative, case 9 from current study was evaluated in CFX and both baffles are in Fig. 8. Results was plotted above: Fig. 9 shows the behavior of Nusselt number; Fig. 10 friction factor and Fig. 11 UA; all of them versus Reynolds number in the annular side of heat exchanger.

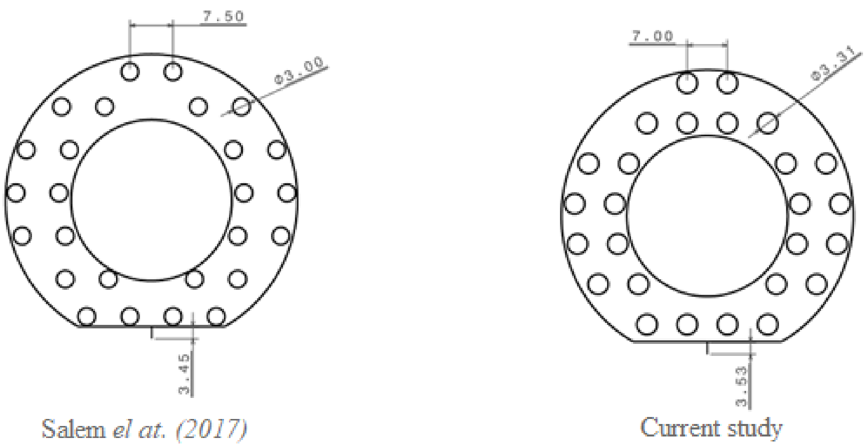

Figure 10. Baffles from case 9 proposed by M. Salem *et al* an current study

All these results are evaluated and have a good comparative of both studies, Nusselt number, friction factor and global coefficient of heat transfer (UA) are showed, respectively, in Figures. 11 to 13.

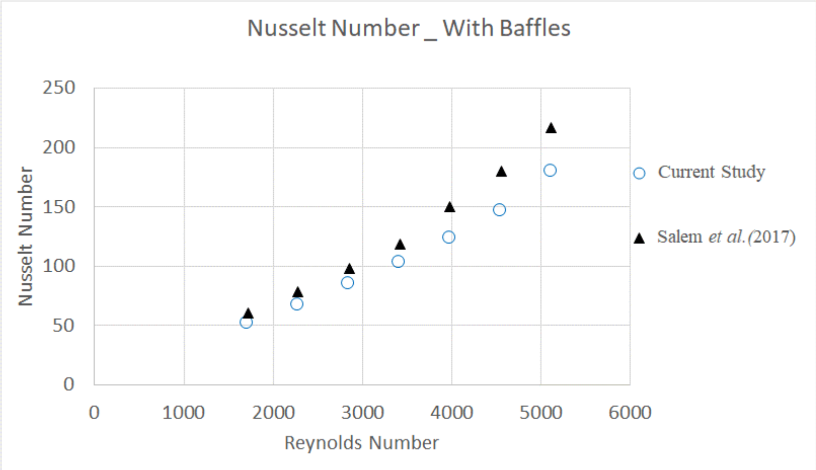

Figure 11. Influence of SSPBs in Nusselt Number.

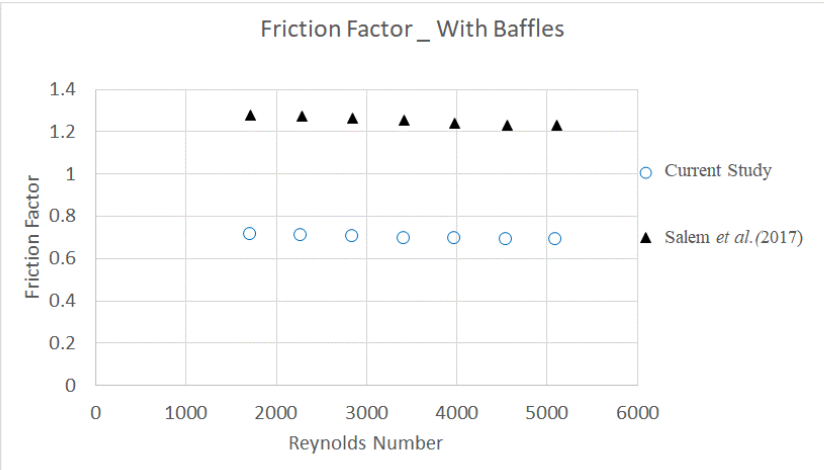

Figure 12. Influence of SSPBs in Friction Factor.

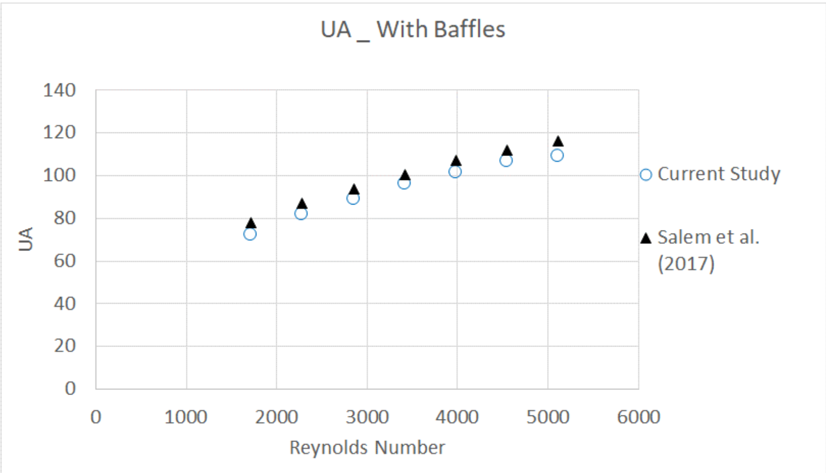

Figure 13. Influence of SSPBs in UA.

Case 9 was investigated numerically and heat transfer characteristics and pressure drop in the annulus of concentric tube heat exchangers with SSPBs were evaluated. In Fig.11 is possible to see that in case 9 from previous studies the Nusselt number and UA are little better than in current study, but even so, TPI which is the objective function, were improved in current study because the pressure drop is much lower when compared to the other cases.

The purpose is to increase the thermal performance index (TPI), which means that the rise in convective heat transfer given due to existing perforated baffles in heat exchangers should be higher than the rise in the fluid pressure drop at same pumping power. So, even losing in heat transfer, the efficiency is improved and compensated due to the gain in friction factor.

4. CONCLUSIONS

The present work is carried out to investigate numerically the heat transfer characteristics and the pressure drop in the annulus of concentric tube heat exchangers with SSPBs. Therefore, eleven cases of baffled heat exchangers of counter-flow configuration are evaluated at different water flow rates. The purpose of increase the thermal performance index (TPI) was reached and the results reveled an improvement for each of the eleven cases studied. To have a comparative, case nine was modeled and CFD analysis proved the accuracy of the numerical study.

Optimized SSPBs showed an improvement in convective heat transfer bigger than the rise in the fluid pressure drop at same pumping power. For some cases, even when heat transfer is worst, the efficiency of heat exchanger could be improved if the pressure drop compensate being slower.

For future work it is proposed to change the project variables ranges using the same correlation of this paper. It may also be proposed to diversify the tube geometric like as length of the heat exchanger, inner diameter annular and outer diameter of tube. Also it is proposed to analyze a new correlations to predict Nusselt number and friction factor.

5. ACKNOWLEDGEMENTS

The last author would like to thank National Council of Scientific and Technologic Development of Brazil - CNPq (Grant numbers: 303906/2015-4-PQ, 405101/2016-3-Univ) for its financial support of this work.

6. REFERENCES

Aicher, T., Kim, W., 1997. Experimental investigation of heat transfer in shell and tube heat exchanger without baffles. *Korean J. Chem. Eng.* Vol. 14 (2), p. 93-100.

Aicher, T., Kim, W., 1998. Experimental investigation of the influence of the cross flow in the nozzle region on the shell-side heat transfer in double-pipe heat exchangers. *Int. Commun. Heat Mass Transf*, Vol. 25 (1), p.43-58.

ANSYS, CFX Modeling Guide, 2012.

ANSYS, CFX SolverTheory Guide, 2012.

Boussaïd, I., Lepagnot, J., Siarry, P., 2013, A survey on optimization metaheuristics. *Information Science*, Vol. 237, p. 82-117.

Das, S., Abraham, A., Chakraborty, U., Konar, A., 2009, Differential evolution using a neighborhood-based mutation operator. *IEEE Trnasactions on Evolutionaty Computation*, Vol. 3, p. 526-553.

Das, S.; Suganthan, P. N, 2011, Differential Evolution: A survey of the State-of-the-Art. *IEEE Transactions on Evolutionary Computation*, Vol. 15, p.4-31.

Donohue, D. A., 1949. Heat transfer and pressure drop in heat exchangers. In *The Lunmus Company, New York 11, N. Y.*

Gao B., Bi Q., Nie Z., Wu J., 2015. Experimental study of effects of baffle helix angle on shell-side performance of shell-and-tube heat exchangers with discontinuous helical baffles. *Experimental Thermal and Fluid Science*, Vol. 68, p. 48–57.

Ghosh, A. Chattopadhyay, S., 2015, Trajectory optimization of satellite launch vechicle using self adaptative differential evolution algorithm, *IEEE Power, Communication and Information Technology Conference* (PCITC), Vol. 1, p. 297-301.

Incropera, F. P., Dewitt, D. P., 2008. *Fundamentals of Heat and Mass Transfer*. 6th, RJ, Brazil: LTC.

Kern, D. Q., 1950. Process Heat Transfer, McGraw-Hill. In *New York, NY, USA*.

Labbadlia, O., Laribi, B., Chetti, B., Hendrick, P., 2017. Numerical Study of the Influence of Tube Arrangement on the Flow Distribution in the Header of Shell and Tube Heat Exchanger. *Applied Thermal Engineering,* Vol. 126, p. 315-321.

Lei, Y., Li, Y., Jing, S., Song, C., Lyu, Y., Wang, F., 2017. Design and performance analysis of the novel shell-and-tube heat exchangers with louver baffles. *Applied Thermal Engineering*, Vol. 125, p. 870-879.

Maakoul, A. E., Laknizi, A., Saadeddine, S., Mutoui, M. E., Zaite, A., Meziane, M., Abdellah, A. B., 2016, Numerical comparison of shell-side performance for shell and tube heat exchangers with trefoil-hole, helical and segmental baffles. *Applied Thermal Engineering*, Vol. 109, p.175–185.

Mellal, M., Benzeguir, R., Sahel, D., Ameur, H., 2017 Hydro-thermal shell-side performance evaluation of a shell and tube heat exchanger under different baffle arrangement and orientation. *International Journal of Thermal Sciences*, Vol. 121, p. 138-149.

Ozden, E., Tari, I., 2010. Shell side CFD analysis of small shell and tube heat exchanger. *Energy Conversion Management* Vol. 51, p. 1004-1014.

Pal, E., Kumar I., Joshi, J. B., Maheshwari, N. K., 2016. CFD simulations of shell-side flow in a shell-and-tube type heat exchanger with and without baffles. *Chemical Engineering Science*, Vol. 143, p. 314-340.

Paul, S.S., Ormiston S. J., Tachie, M. F., 2008. Experimental and numerical investigation of turbulent cross-flow in a staggered tube bundle. *International Journal of Heat and Fluid Flow*, Vol. 29, p.387-414.

Pinto, F. B. Optimization metaheuristics applied to the tuning of the gains of PI controller multivariable,. Master thesis, PUCPR, Curitiba, PR, Brazil.

Remsburg R., 2001. *Thermal design of electronic equipment, electronics handbook series*. *Boca Raton: CRC PRESS LLC.*

Salem, M. R.,Althafeeri, M. K., Elshazly, K. M., Higazy, M. G., Adbraboo, M. F., 2017. Experimental investigation on the thermal performance of a double pipe heat exchanger with segmental perforated baffles. *International Journal of Thermal Sciences*, Vol. 122, p. 39-52.

Standards of the Tubular Exchanger Manufacturers Association. Tarrytown (NY): TEMA Inc.; 2007.

Uzzan, M., Leinen, K. M., Labuza, T. P., 2004. Temperature Profiles within a Double-pipe Heat Exchanger with Countercurrent Turbulent Flow of Newtonian Fluids: Derivation, Validation, and Application to Food Processing. *Journal of Food Science*, Vol 69, p. 433-440.

Wen, J., Yang, H., Wang, S., Gu, X., 2017. PIV experimental investigation on shell-side flow patterns of shell and tube heat exchanger with different helical baffles. *International Journal of Heat and Mass Transfer* Vol. 104, p. 247-25.

Wen, J., Yang, H., Wang, S., Xue, Y., Tong, X., 2015. Experimental investigation on performance comparison for shell-and-tube heat exchangers with different baffles. *International Journal of Heat and Mass Transfer* Vol. 84, p. 990-997.

Yang, J., Liu, W., 2015. Numerical investigation on a novel shell-and-tube heat exchanger with plate baffles and experimental validation. *Energy Conversion and Management*, Vol. 101, p. 689-696.

Yang, J. F., Zeng, M., Wang, Q. W., 2015. Numerical investigation on combined single shell-pass shell-and-tube heat exchanger with two- layer continuous helical baffles. In *International Journal of Heat and Mass Transfer* Vol. 84, p.103-113.

Yang, J. F., Zeng, M., Wang, Q. W., 2016. Numerical investigation on combined multiple shell-pass shell-and-tube heat exchanger with continuous helical baffles. *International Journal of Heat and Mass Transfer*, Vol. 52, p. 1414-1222.

You, Y., Fan, A., Lai, X., Huang, S., Liu, W., 2013. Experimental and numerical investigations of shell-side thermo-hydraulic performances for shell-and-tube heat exchanger with trefoil-hole baffles. *Applied Thermal Engineering*, Vol. 50, p. 950-956.

Zhang, J. F., Li, B., Huang, W. J., Lei, T. G., He Y. L., Tao, W. Q., 2009. Experimental performance comparison of shell-side heat transfer for shell-and-tube heat exchangers with middle-overlapped helical baffles and segmental baffles. In *Chemical Engineering Science*, Vol. 64, p.1643-1653.

Zhou, G. Y., Xiao, J., Zhu, L., Wang, J., Tu, S. T., 2015. A numerical study on the shell-side turbulent heat transfer enhancement of shell-and-tube heat exchanger with trefoil hole baffles. *Energy Procedia*, Vol. 75 p. 3174-3179.

7. RESPONSIBILITY NOTICE

The authors Colaço, Pinto, Batistella, Mariani, Coelho and Salem are the only responsible for the printed material included in this paper.